Monolayer Collapse Regulating Process of Adsorption–Desorption of Palladium Nanoparticles at Fatty Acid Monolayers at the Air–Water Interface

ARTICLE *in* LANGMUIR · FEBRUARY 2011

Impact Factor: 4.46 · DOI: 10.1021/la104822r · Source: PubMed

5 AUTHORS, INCLUDING:

Rodrigo Michelin Iost
University of São Paulo
23 PUBLICATIONS **252** CITATIONS
SEE PROFILE

Frank N Crespilho
University of São Paulo
64 PUBLICATIONS **1,120** CITATIONS
SEE PROFILE

Luciano Caseli
Universidade Federal de São Paulo
81 PUBLICATIONS **1,197** CITATIONS
SEE PROFILE

Langmuir

ARTICLE

pubs.acs.org/Langmuir

Monolayer Collapse Regulating Process of Adsorption−Desorption of Palladium Nanoparticles at Fatty Acid Monolayers at the Air−Water Interface

Thiago E. Goto,[†] Ricardo F. Lopez,[†] Rodrigo M. Iost,[‡] Frank N. Crespilho,[‡] and Luciano Caseli*[,†]

[†]Instituto de Ciências Ambientais, Químicas e Farmacêuticas, Universidade Federal de São Paulo, Diadema, São Paulo 09972-270, Brazil

[‡]Centro de Ciências Naturais e Humanas, Universidade Federal do ABC, Santo André, São Paulo 09210-170, Brazil

ABSTRACT: In this paper, we investigate the affinity of palladium nanoparticles, stabilized with glucose oxidase, for fatty acid monolayers at the air−water interface, exploiting the interaction between a planar system and spheroids coming from the aqueous subphase. A decrease of the monolayer collapse pressure in the second cycle of interface compression proved that the presence of the nanoparticles causes destabilization of the monolayer in a mechanism driven by the interpenetration of the enzyme into the bilayer/multilayer structure formed during collapse, which is not immediately reversible after monolayer expansion. Surface pressure and surface potential−area isotherms, as well as infrared spectroscopy [polarization modulation infrared reflection adsorption spectroscopy (PM-IRRAS)] and deposition onto solid plates as Langmuir−Blodgett (LB) films, were employed to construct a model in which the nanoparticle has a high affinity for the hydrophobic core of the structure formed after collapse, which provides a slow desorption rate from the interface after monolayer decompression. This may have important consequences on the interaction between the metallic particles and fatty acid monolayers, which implies the regulation of the multifunctional properties of the hybrid material.

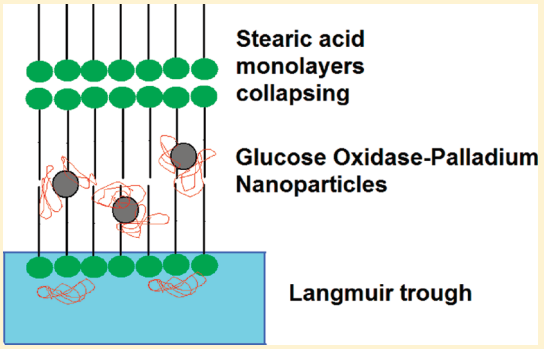

INTRODUCTION

Metallic nanoparticles have been employed for biocatalyst and biosensor construction because of their ability to tailor the properties of several materials, enhancing, for instance, the performance of enzyme-based biocatalytic sensors[1−4] and avoiding enzyme denaturation and the consequent loss of catalytic activity.[5,6] Particularly, when enzymes and nanoparticles are immobilized in ultra-thin films organized at the molecular scale, a high control of the physical properties of the thin film is obtained and a detailed mechanism of the interaction among the molecules can be deeply investigated. Among the so-called ultra-thin films, we highlight those produced by the Langmuir−Blodgett (LB) technique.[7] Langmuir and LB films have been employed to investigate interactions of lipids with biomolecules[8−11] in the process of molecular recognition,[12−14] and in the production of miniaturized devices for sensing, catalysis, and construction of luminescence arrays.[15] For the last case, not only enzymes but also conducting polymers and metallic nanoparticles have been employed.[15−17]

The production of hybrid films with lipids at the air−water interface is a recent well-designed methodology to produce thin films because of the ability of fatty acids and phospholipids to form homogeneous monolayers at the air−water interface. This is not so easy for organic polymers, metallic nanoparticles, and enzymes, because they are generally soluble in water or spread badly on the water surface. Thus, the production of hybrid lipid monolayers with polymers, enzymes, or nanoparticles helps not only to produce the desired materials as a LB film but also to investigate in detail the molecular interaction between the film components and to elaborate the production of new and sophisticated materials to enhance their multifunctional properties. Particularly, the use of mixed nanoparticle−fatty acid monolayers can provide insight into the interaction of "macro-atomic" bodies, such as nanoparticles, albeit capped with organic molecules with a Langmuir monolayer that is undergoing collapse, that is, a 2D−3D transition. It also provides a mechanism to grow hybrid nanostructures very easily, a characteristic of all processes involving Langmuir monolayers.

In this paper, we investigate the interaction of palladium nanoparticles stabilized with glucose oxidase with Langmuir and LB films of fatty acids. We take advantage of the property of each material to produce a hybrid ultra-thin film constituted of palladium, glucose oxidase, and fatty acid. For that, we first carried out a detailed investigation on the interaction of the palladium nanoparticle stabilized with glucose oxidase (GO_x−PdNp) to prove the affinity of the suspension with lipid environments. We may envisage future applications of these films in optical or electronic devices in bioinspired nanostructures for sensing and catalysis.

Received: December 3, 2010
Revised: January 17, 2011
Published: February 11, 2011

MATERIALS AND METHODS

Palladium Nanoparticle Preparation. Enzyme GO_x and ammonium hexachlorum palladate salt $(NH_4)_2PdCl_6$ were purchased from Sigma-Aldrich, and formic acid (98%) was purchased from Vetec. All of the instruments were previously cleaned with ultrapure water and dried before synthesis. GO_x−PdNp nanohybrids were prepared using 1 mL of NH_4PdCl_4 solution (1 mmol/L) added to 1 mL of GO_x (1 mg/mL) and 1 mL of formic acid (1 mmol/L). The final solution was stirred for 1 min and kept in the dark. This reaction occurred for about 45 min. Electronic spectra of GO_x−PdNp solution before and after the synthesis were recorded in an ultraviolet−visible (UV−vis) absorption spectrophotometer (Varian) at 25 °C, in the range of 190−1000 nm, using a 1 cm long quartz curvette. Images of the nanoparticles were obtained using a transmission electron microscope (TEM) (JEOL JEM 2011).

Spreading on the Air−Water Interface. Ultrapure water (resistivity ≈ 18.2 MΩ cm and pH ≈ 5.5−6.0), supplied by a Millipore system, was used as a subphase. Palladium nanoparticles were dispersed in water to render a concentration of 0.3 mg/mL of enzyme as described above. Stearic acid (HSt) from Sigma-Aldrich was dissolved in chloroform to yield a 0.5 mg/mL solution. Aliquots of this solution were spread carefully drop by drop on the surface of the aqueous subphase. After the spreading, an interval delay of 10−15 min for solvent evaporation was predetermined, just before starting the film compression with two movable barriers at a rate of 1.0 $cm^2\ min^{-1}$. For palladium nanoparticle incorporation in the Langmuir trough, aliquots of 10 μL of the suspension were injected just below the interface and left for 30 min until stabilized. The surface pressure and the surface potential were measured during compression using a Wilhelmy plate and a Kelvin probe, respectively, with a KSV mini-trough (system 2, total volume of 220 mL). Polarization modulation infrared reflection absorption spectroscopy (PM-IRRAS) measurements were taken with a KSV PMI 550 instrument (KSV Instrument, Ltd., Helsinki, Finland). The Langmuir trough is set up so that the light beam reaches the monolayer at a fixed incidence angle of 80°. The incoming light is continuously modulated between s and p polarization at a high frequency, which allows for the simultaneous measurement of the spectra for the two polarizations. The difference between the spectra provides surface-specific information, and the sum provides the reference spectrum.[18] With the simultaneous measurements, the effect of the water vapor is largely reduced. All of the experiments were carried out at a constant temperature of 25 ± 1 °C.

Deposition onto Solid Supports. Quartz slides were used as substrates for the transfer of the LB films. The quartz substrates were cleaned by treating with a 5% KOH ethanol solution in an ultrasonic bath for 5 min. The LB film transfer was performed with a dipping rate of 5 mm min^{-1} and a constant surface pressure of 30.0 ± 0.2 mN/m, with the first layer obtained by raising the substrate from the aqueous subphase. For multilayer Y-type LB films, an interval of 10 min was elapsed before the subsequent dipping. In LB films made with hydrophobic plates, quartz slides were previously dipped in tetraethyl orthosilicate (Sigma-Aldrich) for 10 min and then the transfer of the monolayers was initiated by dipping the substrate toward the aqueous subphase. The quality of the LB deposition was first evaluated with transfer ratios in each deposition and then characterized by infrared spectroscopy (PM-IRRAS, KSV Instrument, Ltd., Helsinki, Finland). All LB films were produced at a constant temperature of 25 ± 1 °C and with a deposition rate of 2.0 mm/s.

Experiments in Two Phases. The experiments in two phases were prepared as follows: 0.5 mL of stearic acid solution in chloroform (0.5 mg/mL) and 0.5 mL of GO_x−PdNp aqueous solution (0.3 mg/mL) were mixed rigorously and maintained at room temperature for 5 h. Then, aliquots of 100 μL of each phase were dropped on a gold substrate and dried at room temperature. The main objective of this experiment was to investigate the affinity of GO_x−PdNp for each phase (organic or aqueous). For this, Fourier transform infrared (FTIR) spectroscopy measurements were performed in the transmission mode in the region of 4000−400 cm^{-1} using a Nexus 470 FTIR spectrometer. The spectral resolution was set at 4 cm^{-1}, and 64 scans were added for each spectrum.

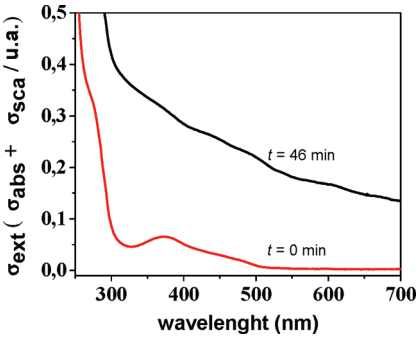

Figure 1. UV−vis electronic spectra of GO_x−PdNp (black line) and 0.5 mmol/L of ammonium hexachloropalladate(IV) (red line).

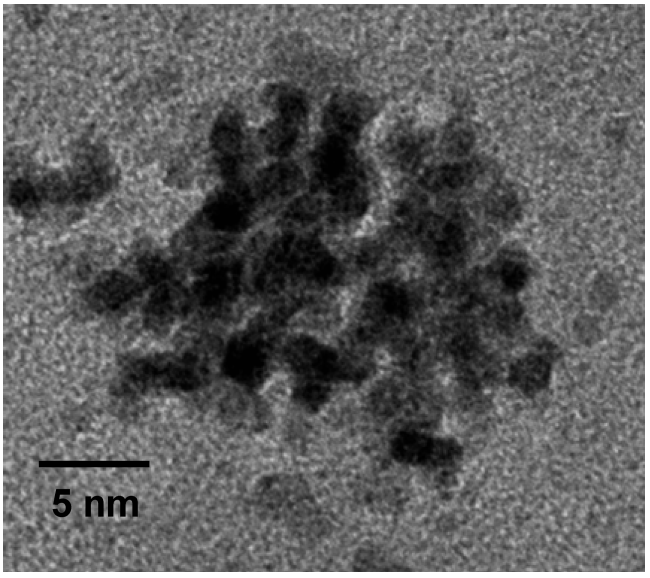

Figure 2. Images of TEM of the GO_x−PdNp nanobiocomposite.

RESULTS AND DISCUSSION

Palladium Nanoparticle Preparation. The synthesis of PdNp in the presence of GO_x molecules caused a change in the color of the solution, and the different stages of the stabilization of the colloidal suspension were observed. The UV−vis electronic spectra for hexachlorum palladate(IV) salt and the GO_x−PdNp bionanocomposite may be observed in Figure 1. Metals of transition series are characterized for electronic transitions because of partially occupied d orbitals. For Pd complexes formed by dissolution in water, a band at about 370 nm is observed. Such electronic transitions can be clearly seen at zero time before formation of PdNps and indicates that Pd^{IV} ions were not consumed totally at the initial time (t = 0). However, the increase of scattering effects during the synthesis clearly indicates the consumption of Pd^{IV} ions, and after 46 min, there is no significant variation of absorbance. Also, it is important to note that the complete consumption of Pd^{IV} salt indicates the formation of the GO_x−PdNp bionanocomposite. The morphology of the nanoparticles was analyzed by TEM images (Figure 2),

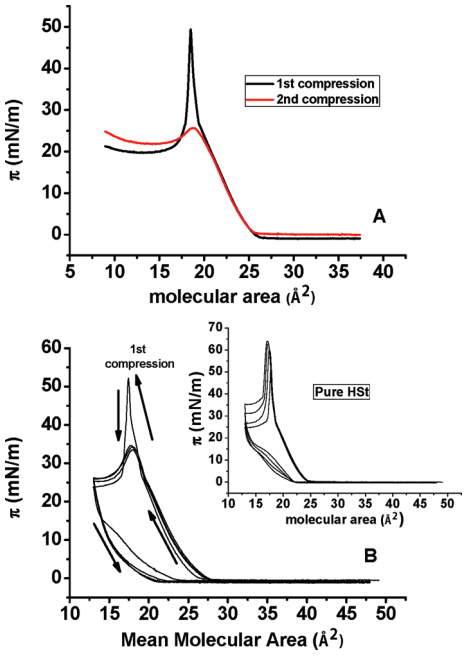

Figure 3. Surface pressure−area isotherm for HSt in the subphase of 200 mL of GO_x−PdNp dispersion (10 μL of 0.3 mg/mL inserted below preformed HSt monolayer at 0 mN/m). Panel A shows the differences between the first and second compressions (carried out after collapse and expansion of the monolayer), and panel B shows successive cycles of compression and decompression of the mixed monolayer. The inset for panel B shows successive cycles of compression−decompression for pure HSt monolayers.

where PdNps adopted spherical structures. In the TEM images, we can clearly observe spherical colloids having a mean diameter of 3.5 nm. Also, no occurrence of precipitates was observed.

Surface Pressure and Surface Potential Isotherms. Figure 3 shows the behavior of a HSt monolayer being compressed upon GO_x−PdNp adsorption. The isotherm shifts to higher molecular areas for monolayers having GO_x−PdNp as the subphase. The minimum area, estimated by taking the most condensed region of the monolayer and extrapolating to zero in terms of surface pressure, is shifted from 18.5 to 20.0 Å^2 when the isotherms for pure HSt and GO_x−PdNp−HSt are compared. This indicates the expansion of the HSt monolayer caused by GO_x−PdNp incorporation. This is expected because the area shift must represent roughly the area occupied by the nanoparticles incorporated in the monolayer. Another phenomenon that can be associated is a possible difficulty to compress HSt monolayers if GO_x−PdNp adsorbs only on the subsurface below the polar heads of the fatty acid.

This type of phenomenon is expected for species being adsorbed at the air−water interface coming from the aqueous subphase, as already reported for proteins,[19] polysaccharides,[20] synthetic polymers,[21] porphirins,[22] liponucleosides,[23] or even small ions,[24] adsorbing at lipid monolayers. Also, it is reported that metallic nanoparticle suspensions expand lipid monolayers, especially for Fe_2O_3 as the subphase for stearic acid.[25] However, the most unusual feature in these results is that, when we perform consecutive compressions for the mixed GO_x−PdNp−HSt monolayers, the collapse pressure decreases significantly, going from 45 to 50 mN/m in the first compression and to 22−26 mN/m for the following compressions (second and third compressions). Successive cycles of

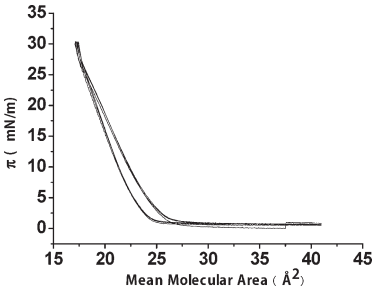

Figure 4. Curves of compression and decompression (3 cycles) for HSt in the subphase of 200 mL of GO_x−PdNp dispersion (10 μL of 0.3 mg/mL inserted below the preformed HSt monolayer at 0 mN/m), with a maximum compression of 30 mN/m.

compression−decompression, whose maximum compression occurred when the collapse had been previously attained (Figure 3B), corroborate with this hypothesis. We have performed compression−decompression cycles up to 10 times, and the behavior of the surface pressure−area isotherm for the compression constantly repeated the profile of the second compression.

The mixed monolayer was also compressed and decompressed several times in a similar way as above, but the maximum compression occurred at a surface pressure below the value corresponding to the monolayer collapse. When a target pressure of 30 mN/m was employed, the curves did not present any meaningful change in the relation to the first compression (Figure 4). This means that the collapse pressure was kept around 45−50 mN/m with successive cycles of compression−decompression. This indicates that this phenomenon, that is, the lower collapse pressure in the second compression, is associated only with the incorporation of GO_x−PdNp during the collapse process in the first compression. The collapse for stearic acid monolayers is described by means of the mechanism of "constant area", in which three molecular layers are formed.[26−28] In this structure, the molecules in the lower layer keep the configuration in which the polar heads are in contact with water molecules in the aqueous subphase and the hydrophobic tails are turned toward the opposite side. The upper layers are then arranged in such a way that a symmetric center is located between the polar heads of the fatty acid molecules that are forming the second and third layers and with tails located on both sides of the heads.[26,27] The decrease of the surface pressure after collapse is attributed to the fact that the surface compression is usually too fast to allow for the accommodation of the amphiphilic molecules above the lower layer, which is preceded by the curvature of the monolayer as a consequence of the overcompression. In this case, the excess of molecules are forced to be expelled from the monolayer, leading to such trilayer structures. If head−head interactions are intermediated by certain divalent cations, trilayers are rapidly formed, leading to a "constant surface pressure collapse".[28] In the case where the monolayer is formed on pure water or on solutions containing only monovalent cations, the formation of the trilayer structure depends upon the capacity of the monolayer to dissociate, which can delay the 2D−3D transition during collapse, resulting in the sudden drop in surface pressure.[26−29] As a result, the growth of 3D nucleation centers is much faster than the compression, which reduces the monolayer surface density forming "craks" or "voids" (patches of bare water surface within the film). Consequently, for the so-called "constant area collapse", there is the formation of coherent sites with layers thicker than three layers with the progress of collapse. The value of surface pressure of collapse for all cases therefore depends upon the

dx.doi.org/10.1021/la104822r |*Langmuir* 2011, 27, 2667–2675

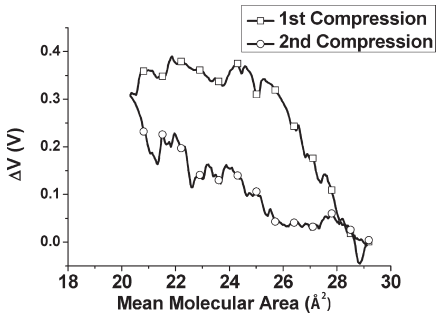

Figure 5. Surface potential−area isotherm for HSt in the subphase of 200 mL of GO_x−PdNp dispersion (10 μL of 0.3 mg/mL inserted below the preformed HSt monolayer at 0 mN/m).

rate of compression, and the liquid-condensed state may not be achieved if the compression is carried out too slow.[27]

Surface potential−area isotherms (Figure 5) show, for mixed GO_x−PdNp−HSt in the first compression, a typical curve with a critical area (onset of the curve, regarding the compression of the monolayer) at about 36−38 Å^2 and a maximum surface potential at about 350−370 mV. There is only a small decrease of this value in relation to the value obtained for pure HSt reported in the literature (about 390 mV).[30] In the second compression, the critical area remains close to that for the first compression. Nevertheless, the values of surface potential between 37 and 27 Å^2 are in general lower than those for the first compression. Only at the collapse, the surface potential values for the first and second compressions are similar. It is likely that the incorporation of GO_x−PdNp provides the distortion of the HSt chains, making the orientation of the dipoles in a vertical position more difficult in relation to the air−water interface plane. A higher amount of GO_x−PdNp or a accommodation of the colloid into the HSt matrix in the second compression must cause a more significant decrease of the surface potential.

PM-IRRAS Study. Figure 6 shows the PM-IRRAS spectra for GO_x−PdNp−HSt mixed monolayers in the region of C−H vibration. Two groups of bands are observed: one centered at 2916 cm^{-1}, corresponding to anti-symmetric stretches for C−H in CH_2 groups, and the other one centered at 2840 cm^{-1}, corresponding to C−H symmetric stretches in CH_2 groups. There are small shifts for both groups of bands to lower energies as long as higher surface pressures are attained. Also, the relative intensity enhances with surface pressure, which can be related to the increase of HSt surface density.

Panel B for Figure 6 shows that both bands (symmetric and anti-symmetric) have their relative intensities increased with surface pressure. However, in the second compression, the relative intensities are lower when compared to those for the first compression. Because the surface density of HSt molecules must be approximately the same, independent if the monolayer is being compressed the first or second time, we attribute this fact to a possible distortion of the alky chains in the second compression, causing a molecular arrangement of the HSt−GO_x−PdNp mixed monolayers. Relative intensities in PM-IRRAS can be attributed to not only the surface density of the materials at the air−water interface but also the orientation of the vibration moment in relation to the interface.[31] Also changes in the surface environment cannot be discarded because of a possible alteration in the refraction index of the monolayer.[31]

Figure 7 shows the PM-IRRAS spectra for the region of amide bands. Because Pd nanoparticles by themselves did not present

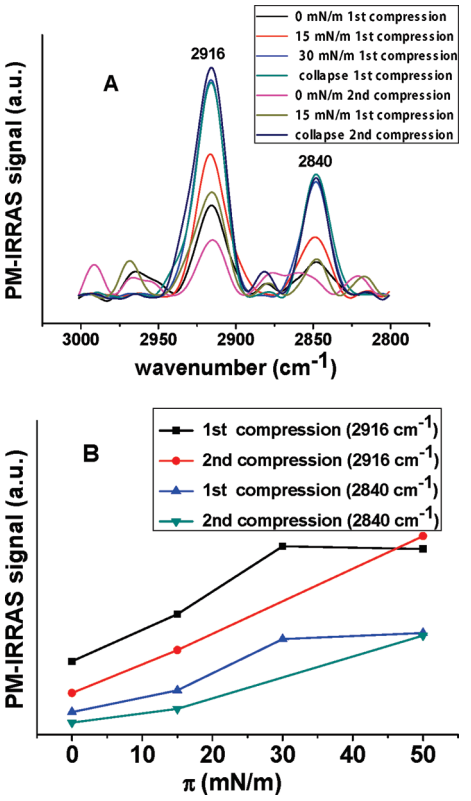

Figure 6. (A) PM-IRRAS spectra for HSt in the subphase of 200 mL of GO_x−PdNp dispersion (10 μL of 0.3 mg/mL inserted below the preformed HSt monolayer at 0 mN/m). (B) Relative intensities of C−H vibrations for HSt in the subphase of 200 mL of GO_x−PdNp dispersion (10 μL of 0.3 mg/mL inserted below the preformed HSt monolayer at 0 mN/m).

significant absorption in the infrared region, we tried to confirm the incorporation of the colloid by analyzing the bands related to the stabilizing agent: the enzyme glucose oxidase. The group of bands at 1510−1570 cm^{-1} is referred to amide II (N−H bend), and the group at 1620−1700 cm^{-1} is referred to amide I (C═O stretch). For PM-IRRAS spectroscopy, bands oriented upward indicate vibration moment oriented roughly parallel to the air−water interface and bands oriented downward indicate vibration moment oriented roughly perpendicular to the air−water interface.[18] In wavenumbers near the regions for amide, bands for OH_2 bending in organized water molecules at the surface may also appear at the 1670−1720 cm^{-1} range.[32]

It is interesting to note that there is inversion in the orientation of the amide I/OH_2 bending bands when we compare the spectrum obtained at 0 mN/m to those obtained at higher surface pressures in the first compression. Also, the band at 1673 cm^{-1} is also shifted to higher energies, reaching the value of 1683 cm^{-1}. The bands that appear as a shoulder at 1642 cm^{-1} (0 mN/m) and 1648 cm^{-1} (other pressures) can be attributed to disordered conformations of GO_x, as already reported in the literature.[33] In the second compression, for all surface pressures, the bands remain in the same orientation as those for the first compression at higher values of surface pressure. All of the results reported thus far lead to the fact that there is a higher incorporation of the complex enzyme−nanoparticle in the lipid monolayer with higher surface pressures, associated with a re-accommodation of the polypeptide moiety into the Langmuir film. Apparently, after

dx.doi.org/10.1021/la104822r |*Langmuir* 2011, 27, 2667–2675

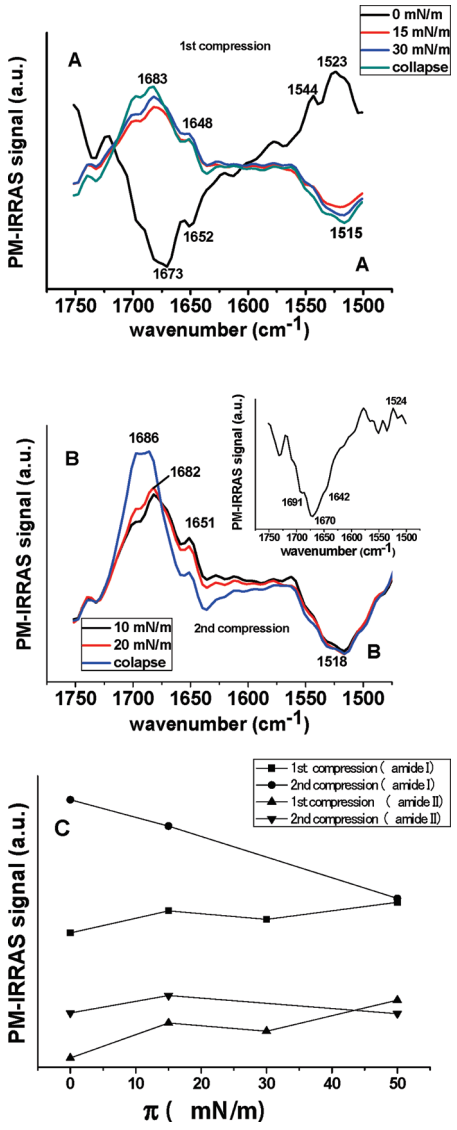

Figure 7. (A and B) PM-IRRAS spectra for HSt in the subphase of 200 mL of GO_x−PdNp dispersion (10 μL of 0.3 mg/mL inserted below the preformed HSt monolayer at 0 mN/m. (C) Relative intensities of amide I and II vibrations for HSt in the subphase of 200 mL of GO_x−PdNp dispersion (10 μL of 0.3 mg/mL inserted below the preformed HSt monolayer at 0 mN/m). For comparison, the inset for panel B shows the PM-IRRAS spectra for GO_x adsorbing at the air−water interface free of lipid or metallic particles.

expansion of the surface after the monolayer collapse, the enzyme does not turn to its original geometrical accommodation. The maximum in 1683 cm^{-1} at 10 mN/m is slightly shifted to higher energies with compression, reaching the value of 1686 cm^{-1} upon collapse. Other shoulders of the band and its width may be associated with CO stretching in β-turn structures, which is usually associated with the interaction of the group with side chains, causing a shift to higher wavenumbers.[34] These bands are overlapped by the OH_2 bending band. The shoulder at 1652 cm^{-1} on the other hand is shifted to lower energies with compression and is associated with the CO stretching in α-helix structures,[35] changing their orientation with compression. We also observe a drastic change in the position of the vibration absorption peaks when compared to a pure GO_x adsorbing at the air−water

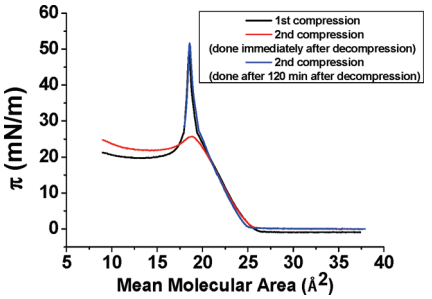

Figure 8. Surface pressure−area isotherm for HSt in the subphase of 200 mL of GO_x−PdNp dispersion (10 μL of 0.3 mg/mL inserted below the preformed HSt monolayer at 0 mN/m). Conditions are specified in the inset.

interface (inset of Figure 7B), in the same conditions for the GO_x−PdNp adsorbing at the air−water interface. The presence of β turns (1681 cm^{-1}), overlapped by the OH_2 bending band (1670 cm^{-1}) and disordered structures (1642 cm^{-1}), is also observed. It is reported in the literature that the presence of lipids at the air−water interface prevents enzymes from denaturing, keeping the secondary structure of the polypeptide moiety unaffected.[9,36,37] This may be occurring in our case, in which the presence of HSt may prevent GO_x from denaturing.

Figure 7C shows that the intensities of both amide I and amide II bands increase with surface pressure in the first compression, pointing to a increasing amount of glucose oxidase−palladium nanoparticle complex at the air−water interface, whose signal is enhanced because of either the increase of surface density or the higher affinity of the material for the HSt monolayer. For the second compression, the bands present higher intensities for both amide I and II. This means that, after one cycle of compression−decompression, a higher amount of GO_x−PdNp remains at the interface and is not redissolved into the aqueous subphase. Therefore, some GO_x−PdNps remain in the monolayer after collapse, which provides the expansion of the monolayer. Also, in the second compression, the infrared intensities seem to go to lower values with compression, especially for amide I bands, which can be related to the desorption of the excess of GO_x−PdNp that occurs even with compression. At higher surface pressures, the relative intensities are apparently close to those obtained in the first compression, indicating that, at this point, a condition close to equilibrium has been reached. Once again, the phenomena associated with these results point to a possible affinity of the GO_x−PdNp with the complex formed by the collapse, attracting a higher amount of nanoparticles, which is not so rapidly desorbed during the decompression of the mixed monolayer after collapse.

Kinetics Effect. To confirm if the high amount of GO_x−PdNps incorporated after collapse is because of a possible slow desorption rate, π−A isotherms for different elapsed times before the second compression were carried out. Figure 8 shows different behaviors for isotherms after two different elapsed times between the first expansion (after attainment of collapse) and the second compression. When the elapsed time was 2 h, the isotherm practically coincides with that obtained in the first compression. This is a new indication that the nanoparticles can be reincorporated in the aqueous subphase after a lag time. However, if this time is not sufficient, the excess of particles still in the monolayer provides the destabilization of the Langmuir film, which causes the lower value of surface pressure for collapse.

dx.doi.org/10.1021/la104822r |*Langmuir* 2011, 27, 2667–2675

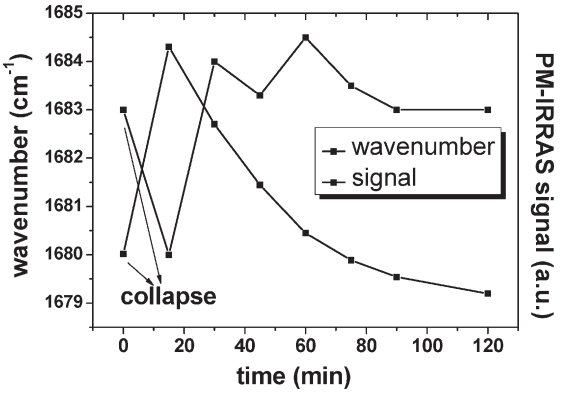

Figure 9. Relative intensities of amide I vibrations for HSt in the subphase of 200 mL of GO_x−PdNp dispersion (10 μL of 0.3 mg/mL inserted below the preformed HSt monolayer at 0 mN/m) at several elapsed times after decompression from the collapse point to the maximum trough area (HSt molecular area of 45 Å^2), except for the value registered in the graph as time zero, related to collapse (HSt molecular area of 15 Å^2).

Figure 9 compares the intensities for amide I bands obtained at several elapse times after one cycle of compression and decompression, with the monolayer compressed to the collapse point in the first compression. For comparison, we also show the intensity of this band in the collapse region (reported in the graph as "zero" for the *x* axis). We note that a significant increase in the intensity values occurs between the collapse and the monolayer freshly decompressed. As long as the monolayer is kept at the maximum trough area, the amide I band intensity decreases, confirming the slow desorption of the nanoparticle after decompression. Wavenumbers for the band centered at 1675−1685 cm^{-1} are also shifted to higher energies with elapsed times, reaching a constant value after 30 min. This indicates that a reaccommodation of the polypeptide moieties remained at the interface at low concentrations, also affecting interfacial water molecules. Probably, low surface density of GO_x−PdNps in the monolayer facilitates the vibration of the OH_2 dipole, increasing the vibration energy.

Looking for a Model: Experiments in Two Phases. Figures 10 and 11 show the FTIR spectra related to the experiment in which organic and aqueous phases of a mixture of $CHCl_3$, stearic acid, GO_x−PdNp, and water were analyzed. Figure 8 shows the spectra for the pure components. For stearic acid, we highlight the bands centered at 2917 and 2843 cm^{-1}, ascribed to C−H stretches for CH_2, and at 1692 cm^{-1}, ascribed to the C═O stretch of the dimer in solid states (which does not exist in the Langmuir monolayer). The band at 1468 cm^{-1} is ascribed to CH_2 deformation. The band at 1301 cm^{-1} is ascribed to CH_2 twist. The band at 943 cm^{-1} is ascribed to C−OH deformation. For GO_x−PdNp, we observe the amide I (C═O stretch) band, which is centered at 1687 cm^{-1}, and the amide III (C−N stretch) band in α-helix structures, which is centered at 1293 cm^{-1}. Also, we observe bands at 1157 and 1044 cm^{-1} (C−N stretch) and at 999 cm^{-1} (ring vibrations for tryptophan). Therefore, the bands attributed to stearic acid are stronger in the organic phase, and the main bands for GO_x−PdNp are present mainly in the organic phase. This proves that the mechanism in which stearic acid sequesters the nanoparticles is driven by the affinity between GO_x−PdNp and the alkyl chains of HSt. Maybe HSt polar heads contribute to the mechanism as the first step to incorporate the nanoparticles in the monolayer structure, and as

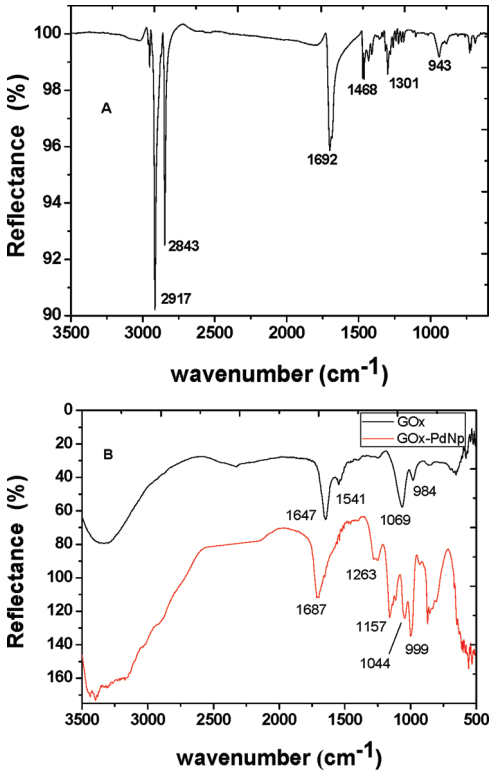

Figure 10. FTIR spectra for stearic acid and GO_x (pure solution or as stabilizing agent for GO_x−PdNp).

a result, during the collapse, the nanoparticle must penetrate into the bilayer structure formed during the collapse (or multilayer structures, as defended for HSt[26−29]).

Looking for a Model: Role of GO_x. To better identify the separated influence of GO_x and palladium in this mechanism, surface pressure−area isotherms were obtained for glucose oxidase without the presence of GO_x−PdNps (not shown) and also for palladium stabilized by poly(styrenesulfonate) (PSS) (not shown). For both cases, the collapse decreased to surface pressures below 30 mN/m for the immediate second compression. However, for PSS−PdNp, the surface pressure values remained constant after collapse, and for GO_x, the surface pressure decreased to an equilibrium value (around 20 mN/m), as for that observed for GO_x−PdNp. This indicates that the driving factor to reduce the collapse is the stabilizing agent by itself, GO_x or PSS. However, because the collapse presents different profiles, the intrinsic interaction between GO_x and PdNp must determine not only the surface pressure of collapse but also the decrease of the surface pressure after its attainment. Figure 12 shows the spectra for GO_x (without palladium) in stearic acid monolayers. Basically, the position of the bands for C−H stretches did not change significantly (panel A). Also, in Figure 12B, the intensities of the bands increased with surface pressure, as expected. However, when the intensities obtained in the first, second, and third compressions are compared, there is no significant alteration in the values of intensities as observed for GO_x−PdNp for amide I bands (inset for panel C). The bands presented similar behavior to those for GO_x−PdNp, indicating that the enzyme must be present at the air−water interface in higher amounts upon decompression. The unique relevant difference between the sample with and without palladium is that, for GO_x−PdNp, there is a significant decrease in the C−H

dx.doi.org/10.1021/la104822r |*Langmuir* 2011, 27, 2667–2675

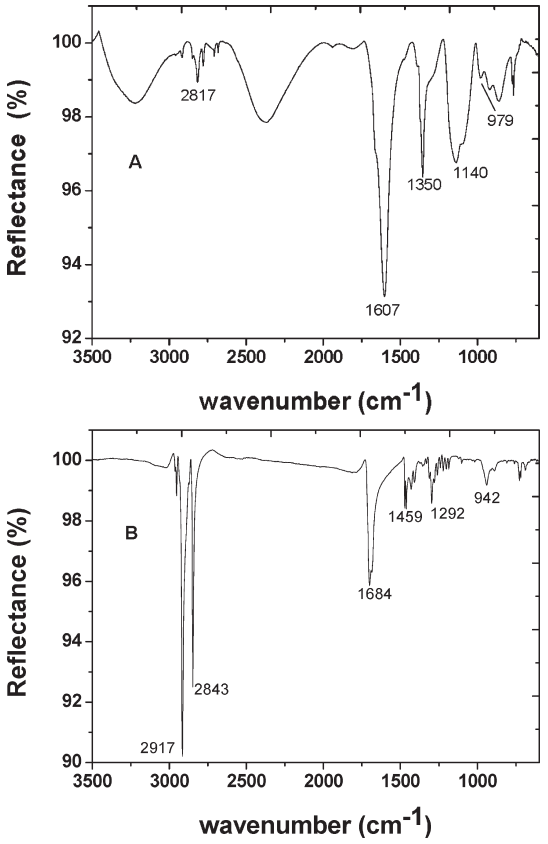

Figure 11. FTIR spectra for the mixture of $HCCl_4$ + stearic acid + GO_x−PdNp + water: (A) spectrum for the aqueous phase and (B) spectrum for the organic phase.

stretches that did not occur when only GO_x is present as the subphase solution for the HSt monolayer. Then, the metallic nanoparticle must interact strongly with stearic acid at the air−water interface, causing the decrease in the C−H signal for the subsequent compression. This fact can be related to a couple of factors: (i) GO_x−PdNp can cause the removal of some fatty acid molecules from the air−water interface and takes them to the aqueous subphase, which may cause the decrease of the PM-IRRAS signal for the subsequent compressions; (ii) the multilayer structure formed during collapse can have disordered arrangements, enhanced during decompression. As it is formed, an anisotropic region at the interface, which is not instantly unform, the PM-IRRAS signal, sensitive only to anisotropic regions, such as surfaces in general, may decrease significantly.

Also, the presence of bands for β-turn/OH_2 bending centered at 1678 cm^{-1} and other well-defined bands for β-sheet structures (1620 cm^{-1}) and shoulders at 1654 and 1692 cm^{-1} indicates the fraction of the polypeptide at α-helix and β-sheet structures.[34] This reveals that the interaction of palladium has a relevant role in keeping the structure of the enzyme.

Looking for a Model: Deposition as LB Films. For a better understanding of the effect of each component of the GO_x−PdNp system interacting with stearic acids, we transferred the mixed monolayers from the air−water interface to solid supports through four strategies: (i) one layer from the mixed GO_x−PdNp−HSt monolayer was transferred as LB film, with the plate emerging from the subphase (upstroke deposition) at a surface pressure of 30 mN/m; (ii) two layers from the mixed GO_x−PdNp−HSt monolayer were transferred as Y-LB film at a surface

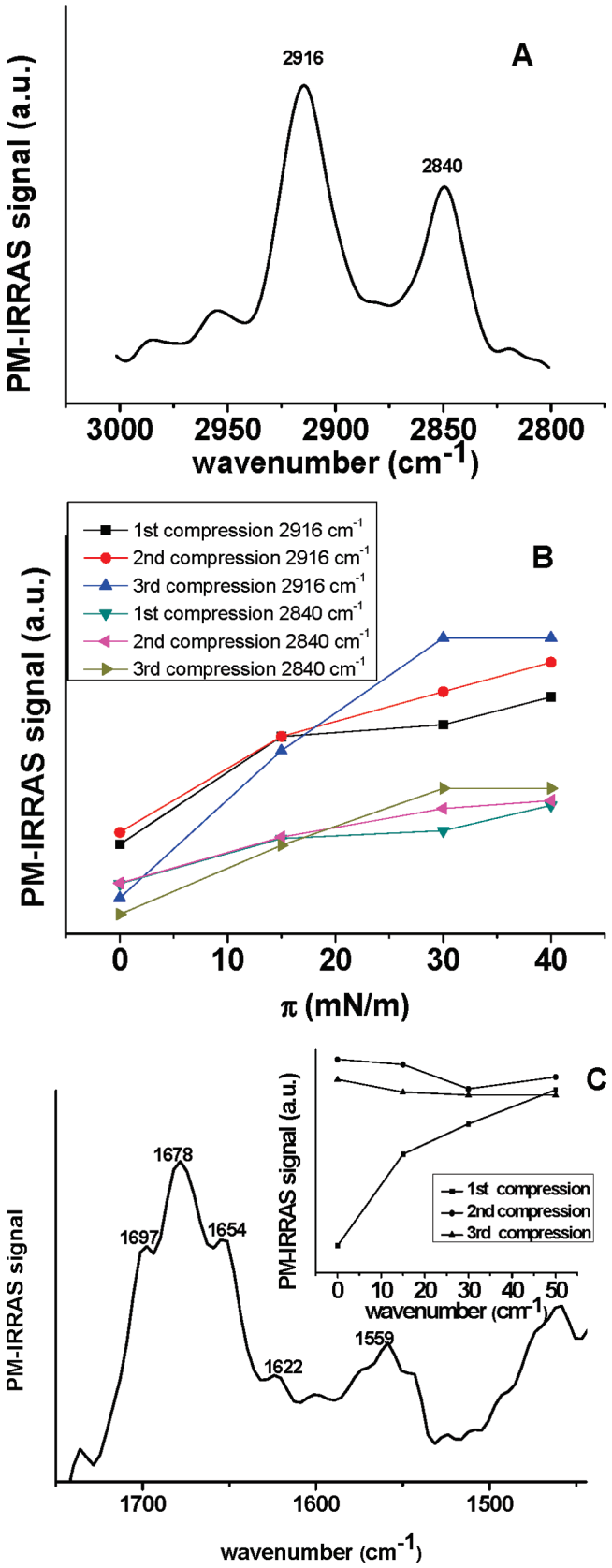

Figure 12. PM-IRRAS spectra for HSt in the subphase of 200 mL of glucose oxidase (10 μL of 0.5 mg/mL inserted below the preformed HSt monolayer at 0 mN/m). Panel A represents the C−H vibration region, and panel B represent the amide I and II regions.

dx.doi.org/10.1021/la104822r |*Langmuir* 2011, 27, 2667–2675

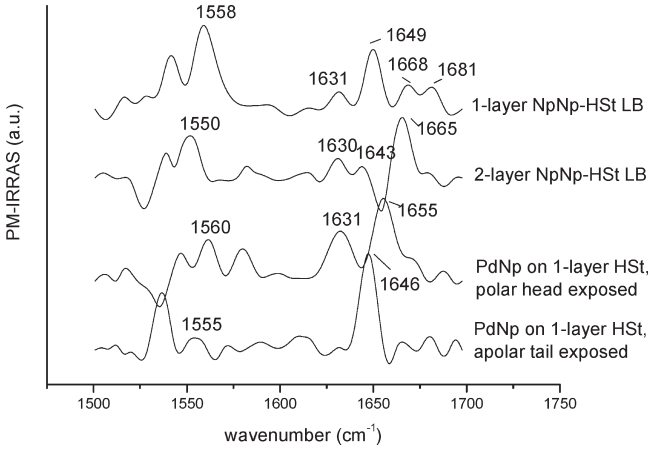

Figure 13. PM-IRRAS for HSt-Np LB films transferred at 30 mN/m.

pressure of 30 mN/m, with the first layer emerging from the subphase (upstroke deposition); (iii) a preformed one-layer HSt LB film, deposited with a hydrophobic plate immerging in the subphase, was in the sequence dipped in a GO_x−PdNp suspension contained in a separated sample (in the same concentration as in the subphase for the monolayer experiments) and left for 10 min until removal of the plate; and (iv) a preformed one-layer HSt LB film, deposited with the hydrophilic plate emerging from the subphase, was dipped in the GO_x−PdNp suspension (in the same concentration as in the subphase for the monolayer experiments) and left for 10 min until removal of the plate. For the films made from the first two strategies, the objective was to check if GO_x−PdNp had affinity specifically with the monolayer itself or with the bilayer (or multilayer) structure probably formed in collapse processes.[26−28] For the third and forth strategies, the objective was to verify the affinity of GO_x−PdNp with the polar heads or with the hydrophobic tails of HSt, given that these groups were alternately exposed to the solution containing the nanoparticle.

In Figure 13, we show that the amide I region has in all cases intense bands, but with different wavenumber positions. For films produced with one layer deposited from mixed GO_x−PdNp−HSt monolayers, the band at 1649 cm^{-1}, which points to disordered structure conformations, may be related to the interaction of GO_x with hydrophilic groups of HSt. Bands at 1631, 1668, and 1681 cm^{-1} indicate an extended chain β-sheet band and also β turns. When GO_x−PdNp is adsorbed from aqueous solution directly onto hydrophilic polar heads of HSt, an extended chain β-sheet band is kept at 1631 cm^{-1} but a band at 1655 cm^{-1} appears, indicating a protein conformation in α-helix structures. For LB films with two layers, the probable adsorption of the enzyme into the bilayer matrix leads to a higher shift of the main amide I band to 1665 cm^{-1}. However, the onset for 1643 cm^{-1} (α helix) is an indication that the main axis of the α helix is changing its orientation in relation to the plane of the lipid film. An extended chain β-sheet band is kept at 1630−1631 cm^{-1}. This indicates that the adsorption of GO_x in this kind of polar matrix may alter the conformation of the enzyme. For one-layer-preformed HSt LB film, where the GO_x−PdNp probably does not have the opportunity to incorporate into a bilayer structure, the nanoparticle may be entrapped between the lipid and the solid substrate, with some segments interacting with the alkyl chains of HSt. For this film, there is a well-defined band, related to disordered structures in 1649 cm^{-1}. Amide II bands are also present in different positions and deconvolutions depending upon the strategy

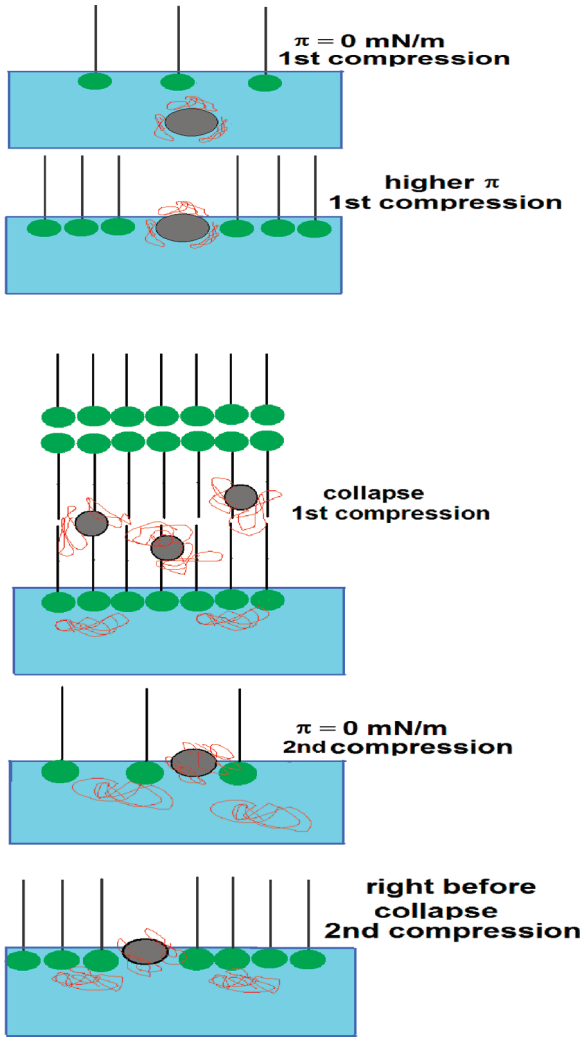

Figure 14. Model for nanoparticles of palladium stabilized with glucose oxidase adsorbing at stearic acid monolayers.

employed. Basically, we can conclude that the environment provided to the enzyme influences the secondary conformation of the polypeptide chain, which may imply key consequences in its functional properties.

Then, on the basis of the results reported thus far, we propose a model (visualized in Figure 14), in which the collapse process regulates the process of adsorption−desorption of palladium nanoparticles at fatty acid monolayers at the air−water interface: (1) As long as high surface densities of HSt are reached, higher amounts of GO_x−PdNps are incorporated into the monolayer, indicating affinity between HSt and GO_x−PdNp. (2) The multilayer structure of collapse promotes a higher incorporation of GO_x−PdNp at the air−water interface, probably entrapped in the inner hydrophobic structure formed. (3) After monolayer decompression, GO_x−PdNp desorbs slowly from the interface. However, if new compression is carried out before complete desorption, the excess of GO_x−PdNp still incorporated destabilizes the HSt monolayer, which is reflected in the low collapse surface pressure. (4) The environment of collapse provided to GO_x−PdNp enables specific hydrophobic and hydrophilic interactions because of the thickness of the layer. Therefore, the incorporation of GO_x−PdNp in the hydrophobic structure in

dx.doi.org/10.1021/la104822r |*Langmuir* 2011, 27, 2667–2675

the inner bilayer will determine the secondary structure of the enzyme entrapped in this new and original hybrid structure.

These results as a whole are important because they not only prove the affinity of the nanoparticle with fatty acids but also help to understand interactions of molecules and particles in the subphase with the monolayer at the collapse. With this present work, we may envisage the hybrid materials produced with fatty acid and metallic nanoparticle stabilized by glucose oxidase to multifunctional materials with enhanced properties for sensors, catalysts, and organic and inorganic devices.

CONCLUSIONS

In this paper, we have exploited the affinity of palladium nanoparticles stabilized with glucose oxidase with fatty acid monolayers at the air−water interface. The presence of the nanoparticles decreased the stability of the Langmuir film in the sense that the collapse was reduced to lower surface pressures during the second cycle of compression when collapse has been previously attained. This fact was attributed to the slow desorption of the nanoparticle after decompression. If a longer time is imposed to the monolayer to relax after decompression, no unstable monolayer (low collapse pressure) is observed anymore. Infrared spectroscopy applied in several conditions of incorporation of the nanoparticles in the fatty acid films shows that the environment imposed to the enzyme may drive its secondary structure, conformation, and orientation. This may have important consequences on the interaction between the metallic particles, the fatty acid, and the enzyme employed in this present work, which may help to regulate the multifunctional properties of the hybrid material.

AUTHOR INFORMATION

Corresponding Author

*E-mail: lcaseli@unifesp.br.

ACKNOWLEDGMENT

We gratefully acknowledge the financial support from FAPESP (Frank N. Crespilho, Project Number 2009/15558-1), CAPES, CNPq, Instituto Nacional de Eletrônica Orgânica (INEO), and Rede NanoBioMed−Brasil (CAPES). Luciano Caseli's research is supported by FAPESP (Grant 2008/10851-0). Thiago E. Goto received a scholarship from CAPES−Nanobio. Ricardo F. Lopez received a scholarship from FAPESP (20010/07248-0). The authors are also indebted to Professor Welter C. Silva for help with the TEM images.

REFERENCES

(1) Ahmad, M. Z.; Akhter, S.; Jain, G. K.; Rahman, M.; Pathan, S. A.; Ahmad, F. J.; Khar, R. K. *Expert Opin. Drug Delivery* **2010**, *7*, 927–942.
(2) Willner, I.; Basnar, B.; Willner, B. *FEBS J.* **2007**, *2*, 302–309.
(3) Crespilho, F. N.; Zucolotto, V.; Brett, C. M. A.; Oliveira, O. N., Jr.; Nart, F. C. *J. Phys. Chem. B* **2006**, *110*, 17478–17483.
(4) Rao, C. R. K.; Trivedi, D. C. *Catal. Commun.* **2006**, *7*, 662–668.
(5) Jv, Y.; Li, B. X.; Cao, R. *Chem. Commun.* **2010**, *46*, 8017–8019.
(6) Dong, J.; Wen, Y.; Miao, Y.; Xie, Z. J.; Zhang, Z. R.; Yang, H. F. *Sens. Actuators, B* **2010**, *150*, 141–147.
(7) Blodgett, K. B. *J. Am. Chem. Soc.* **1934**, *56*, 495–495.
(8) Girard-Egrot, A. P.; Godoy, S.; Blum, L. J. *Adv. Colloid Interface Sci.* **2005**, *116*, 205–225.
(9) Siqueira, J. R., Jr.; Caseli, L.; Crespilho, F. N.; Zucolotto, V.; Oliveira, O. N., Jr. *Biosens. Bioelectron.* **2010**, *25*, 1255–1264.
(10) Pavinatto, F. J.; Caseli, L.; Oliveira, O. N., Jr. *Biomacromolecules* **2010**, *11*, 1897–1908.
(11) Brockman, H. *Curr. Opin. Struct. Biol.* **1999**, *9*, 438–443.
(12) Leblanc, L. M. *Curr. Opin. Struct. Biol.* **2006**, *10*, 529–536.
(13) Baszkin, A. *Adv. Colloid Interface Sci.* **2006**, *128*, 111–120.
(14) Ariga, K.; Nakanishi, T.; Michinobu, T. *J. Nanosci. Nanotechnol.* **2006**, *6*, 2278–2301.
(15) Mallick, K.; Witcomb, M. *Platinum Met. Rev.* **2007**, *51*, 3–15.
(16) Santos, T. C. F.; Peres, L. O.; Wang, S. H.; Oliveira, O. N.; Caseli, L. *Langmuir* **2010**, *26*, 5869–5875.
(17) Shipway, A. N.; Katz, E.; Willner, I. *Chem. Phys. Chem.* **2000**, *1*, 18–52.
(18) Buffeteau, T.; Desbat, D.; Turlet, J. M. *Appl. Spectrosc.* **2010**, *45*, 380–389.
(19) Caseli, L; Moraes, M. L.; Zucolotto, V.; Ferreira, M.; Nobre, T. M.; Zaniquelli, M. E. D.; Rodrigues, U. P.; Oliveira, O. N., Jr. *Langmuir* **2006**, *22*, 8501–8508.
(20) Pavinatto, F. J.; Pacholatti, C. P.; Montanha, E. A.; Caseli, L.; Silva, H. S.; Miranda, P. B.; Viitala, T.; Oliveira, O. N., Jr. *Langmuir* **2009**, *17*, 10051–10061.
(21) Caseli, L.; Nobre, T. M.; Low, W.; Zaniquelli, M. E. D. *Colloid Surf., B* **2001**, *22*, 309–321.
(22) Caseli, L.; Vinhado, F. S.; Iamamoto, Y.; Zaniquelli, M. E. D. *Colloid Surf., A* **2003**, *229*, 169–180.
(23) Montanha, E. A.; Pavinatto, F. J.; Caseli, L.; Kaczmarek, O.; Liebscher, J.; Huster, D.; Oliveira, O. N., Jr. *Colloid Surf., A* **2010**, *77*, 161–165.
(24) Silva, R. F.; Zaniquelli, M. E. D.; Serra, O. A.; Torriani, I. L.; de Castro, S. G. C. *Thin Solid Films* **1998**, *324*, 245–252.
(25) Degen, P.; Paulus, M.; Maas, M.; Rainer, K.; Schmacke, S.; Struth, B.; Metin, T.; Rehage, H. *Langmuir* **2008**, *24*, 12958–12962.
(26) Kundu, S.; Datta, A.; Hazra, S. *Phys. Rev. E: Stat. Phys., Plasmas, Fluids, Relat. Interdiscip. Top.* **2006**, *73*, No. 051608.
(27) Rabinovitch, W.; Robertson, R. F.; Mason, S. G. *Can. J. Chem.* **1960**, *10*, 1881–1890.
(28) Kundu, S.; Langevin, D. *Colloid Surf., A* **2008**, *325*, 81–85.
(29) Kundu, S.; Datta, A.; Hazra, S. *Langmuir* **2005**, *21*, 5894–5900.
(30) Oliveira, O. N., Jr.; Taylor, D. M.; Morgan, H. *Thin Solid Films* **1992**, *1−2*, 76–78.
(31) Buffeteau, T.; Blaudez, D.; Perez, E.; Besbat, B. *J. Phys. Chem. B* **1999**, *24*, 5020–5027.
(32) Ulrich, W. P.; Voegel, H. *Biophys. J.* **1999**, *76*, 1639–1647.
(33) Haouz, A.; Twist, C.; Zentz, C.; Tauc, P.; Alpert, B. *Eur. Biophys.* **1998**, *27*, 19–25.
(34) Orbulescu, J.; Micic, M.; Ensor, M.; Trajkovic, S.; Daunerst, S.; Leblanc, R. M. *Langmuir* **2010**, *26*, 3268–3274.
(35) Blaudez, D.; Boucher, F.; Buffeteau, T.; Desbat, B.; Grandbois, M.; Salesse, C. *Appl. Spectrosc.* **1999**, *53*, 1299–1304.
(36) Schmidt, T. F.; Caseli, L.; Viitala, T.; Oliveira, O. N. *Biochim. Biophys. Acta, Biomembr.* **2008**, *1778*, 2291–2297.
(37) Goto, T. E.; Lopez, R. F.; Oliveira, O. N., Jr.; Caseli, L.; Oliveira, O. N. *Langmuir* **2010**, *26*, 11135–11139.